Nanoscale

PAPER

View Article Online
View Journal | View Issue

Cite this: *Nanoscale*, 2018, **10**, 18728

Magnetization dynamics induced by the Rashba effect in ferromagnetic films†

Zhizhou Yu,[a] Jian Chen,[b] Lei Zhang,[c] Yanxia Xing[d] and Jian Wang*[b]

Manipulating the magnetization of ferromagnets by the current-induced spin–orbit torque has great potential application in the design of low energy consumption spintronic devices. Normally, an external magnetic field is needed for the reversal of current assisted magnetization by the spin–orbit torque. Recently, the switching of magnetization driven by the spin–orbit torque in the absence of an external magnetic field was reported in a $Ta/Co_{20}Fe_{60}B_{20}/TaO_x$ system with lateral structural asymmetry. To understand the physics behind this experiment, we performed first principles calculations on the potential profile at the interface between the ferromagnetic film and the wedge-shaped deposited metal oxide in the Ta/Co/TaO system. This revealed that the lateral structural asymmetry generates two additional Rashba interactions which can reduce the minimum external field required to reverse the magnetization. In addition, we derived the Landau–Lifshitz–Gilbert equation from a quantum transport perspective and numerically investigated the magnetization dynamics in ferromagnetic films induced by Rashba interactions including those generated by lateral asymmetry. Our theoretical simulation provides microscopic explanations of experimental observations of magnetization switching in the absence of an external field of devices with lateral structural asymmetry.

Received 7th June 2018,
Accepted 11th September 2018

DOI: 10.1039/c8nr04628j

rsc.li/nanoscale

1. Introduction

Magnetization switching of spintronic devices is the key to read or write information in memories and logic circuits. Instead of traditional external magnetic fields, the spin torque generated by local electric currents has opened a new pathway to efficiently control magnetization since the discovery of spin transfer torque. This has accelerated the development of high-performance data storage devices and has reduced energy consumption.[1–3] Spin transfer torque originates from the transfer of local spin angular momentum between a pinned and a free ferromagnet separated by a thin insulator.[4] Recently, an alternative way to produce spin torque by the spin–orbit coupling in ferromagnetic layers lacking structural inversion symmetry has been proposed theoretically[5–8] and realized experimentally.[9–17] Such spin–orbit torque is induced by the nonequilibrium spin polarization of conduction electrons due to s–d exchange interactions.[5]

The pioneering experiments of magnetization switching on $AlO_x/Co/Pt$ heterostructures by current-induced spin–orbit torque have shown that the in-plane current injection induces transverse spin accumulation since the conduction electrons experience an effective field $\mathbf{H}_R = \alpha_R(\mathbf{j} \times \hat{z})$ from the Rashba interactions, where α_R is the Rashba constant, $\mathbf{j}$ is the unit vector of the in-plane current density and $\hat{z}$ is the perpendicular unit vector.[9,10] Indeed, an effective switching field orthogonal to the directions of both the magnetization and the Rashba field $\mathbf{H}_R$ was observed. The switching of magnetization by spin–orbit torque has also been studied in symmetric structures such as Pt/ferromagnet/Pt, in which the spin Hall effect is dominant for current-induced switching.[18] In these experiments, an in-plane external magnetic field along the current direction was required for the deterministic switching of magnetization. Recently, the switching of the magnetization of $Ta/Co_{20}Fe_{60}B_{20}/TaO_x$ driven by spin–orbit torque in the absence of an external magnetic field was reported by introducing lateral structural asymmetry which may generate an additional perpendicular field-like spin–orbit torque when current flows through the device.[15] Moreover, field-free switching of magnetization has been realized in antiferromagnetic/ferromagnetic/oxide structures,[19] and also observed in hybrid ferromagnetic/ferroelectric structures by using the electric field produced in substrates to control the spin–orbit torque.[20]

[a]*Center for Quantum Transport and Thermal Energy Science, School of Physics and Technology, Nanjing Normal University, Nanjing 210023, China*
[b]*Department of Physics and the Center of Theoretical and Computational Physics, The University of Hong Kong, Hong Kong, China. E-mail: jianwang@hku.hk*
[c]*State Key Laboratory of Quantum Optics and Quantum Optics Devices, Institute of Laser Spectroscopy and Collaborative Innovation Center of Extreme Optics, Shanxi University, Taiyuan 030006, China*
[d]*Department of Physics, Beijing Institute of Technology, Beijing 100081, China*

†Electronic supplementary information (ESI) available: The tight-binding Hamiltonian, derivation of the stochastic LLG equation, and the time-dependent Green's function in instantaneous representation. See DOI: 10.1039/C8NR04628J

Despite intensive experimental studies, most of the theoretical investigations based on the Landau–Lifshitz–Gilbert (LLG) equation treat the magnetization dynamics on a semiclassical level.[21–25] It was shown that the Rashba interactions can generate an intrinsic torque, namely, the spin–orbit torque in the LLG equation, due to a nonequilibrium spin density.[5,6] Based on the LLG equation, the macrospin simulation[23] shows magnetization switching in ferromagnetic films with perpendicular anisotropy which agrees well with experimental observations.[10] However, it is not quite clear to what extent the semiclassical macrospin description based on the LLG equation remains valid for ultrafast magnetization switching of nanostructures. Moreover, the magnetization dynamics with structural asymmetry can only be explained by considering additional torques in the LLG equation whose mechanisms are still not clear.[15] Therefore, a quantum theory to understand the spin–orbit torque in a system with Rashba interactions is essential to study the magnetization dynamics in nanomagnets.

In this paper, we have developed a stochastic LLG equation using the non-equilibrium Green's function technique from the perspective of quantum transport and study the magnetization dynamics due to the spin–orbit torque of ferromagnetic films. In order to understand the effect of wedge-shaped metal oxide on the magnetization switching, two different types of Rashba interactions are proposed due to the potential profile at the interface between the metal oxide and the ferromagnetic film obtained from first-principles calculation. Both of them can reduce the minimum external field along the current direction required for deterministic magnetization switching, and this provides physical explanations for the experimental observations of field-free magnetization switching due to lateral structural asymmetry.

2. Computational methods

The device we propose consists of a 2 nm × 2 nm cobalt film sandwiched between two semi-infinite normal leads, as shown in Fig. 1(a). An external magnetic field B_y along the y-axis was applied. The initial localized magnetization is assumed to slightly deviate from the z-axis with $\theta = 5°$ and $\phi = 0°$. The dynamics of magnetization are governed by the following stochastic LLG equation which was obtained using the non-equilibrium Green's function formalism from the perspective of quantum transport (see detailed derivation in ESI†)

$$\frac{\mathrm{d}\mathbf{m}}{\mathrm{d}t} = -\mathbf{m}\times\left[J\mathbf{s}_{\mathrm{C}} + \gamma\mathbf{B} + \frac{\gamma}{M}\partial_{\mathbf{m}}U^{\mathrm{ani}}(\mathbf{m})\right]. \quad (1)$$

Here, $\mathbf{m}$ is the magnetization unit vector. J is the exchange interaction describing the coupling of the electron levels with the magnetization, γ is the gyromagnetic ratio of the localized spin, $\mathbf{B}$ is the external magnetic field, U^{ani} is the uniaxial anisotropy, M is the magnetization saturation magnitude, and $\mathcal{V}$ is the system volume. The first term of the RHS of eqn (1) is proportional to the current induced spin–orbit torque. The total electron spin is $\mathbf{s}_{\mathrm{C}} = \mathbf{s}_{\mathrm{C}}^{(0)} + \mathbf{s}_{\mathrm{C}}^{(1)}$ of which the two components are given by

$$\boldsymbol{s}_{\mathrm{C}}^{(0)} = -\frac{i}{2}\int\frac{\mathrm{d}E}{2\pi}\mathrm{Tr}[\boldsymbol{\sigma}G_{\mathrm{f}}^{<}], \quad (2)$$

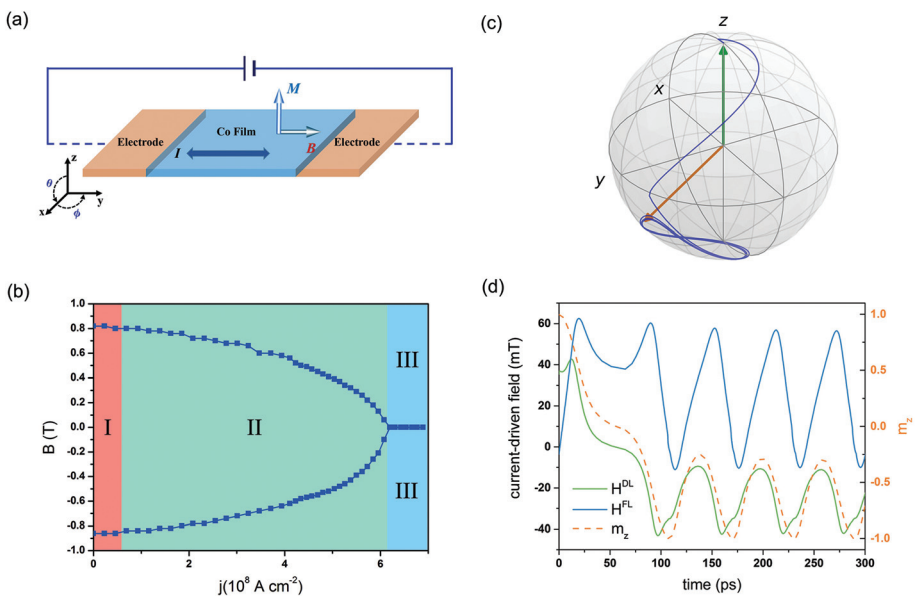

Fig. 1 (a) Schematic diagram of a Co film connected with two semi-infinite leads. (b) Phase diagram of the magnetization switching with different external magnetic fields and current densities. Region I: External field-induced reversal. Region II: Reversal induced by both the external field and current-induced spin–orbit torque. Region III: Current-induced reversal. (c) Motion of magnetization switching (blue line) in the presence of both a current and a magnetic field with $j = 5.5 \times 10^8$ A cm^{-2} and $B_y = 0.4$ T. The green and orange arrows indicate the initial and final magnetization, respectively. (d) Time-dependence of the current-induced field-like and damping-like effective field, and the z-component of the magnetization m_z.

and

$$\boldsymbol{s}_{\mathrm{C}}^{(1)} = \frac{J}{2}\left(\frac{M}{\gamma}\right)\int \frac{\mathrm{d}E}{2\pi}\mathrm{ReTr}[G_{\mathrm{f}}^{a}G_{\mathrm{f}}^{a}\boldsymbol{\sigma}G_{\mathrm{f}}^{<}\boldsymbol{\sigma}]\cdot\dot{\boldsymbol{m}}, \quad (3)$$

respectively. In the above, $G_{\mathrm{f}}^{r(a)}$ and $G_{\mathrm{f}}^{<}$ are the frozen retarded (advanced) and lesser Green's functions in the adiabatic limit, respectively. Here, $\mathbf{s}_{\mathrm{C}}^{(0)}$ and $\mathbf{s}_{\mathrm{C}}^{(1)}$ are the zero-order and first-order terms of $\mathbf{s}_{\mathrm{C}}$ with respect of time, respectively. σ is the Pauli matrix, and $\hat{\mathbf{m}} = \mathrm{d}\mathbf{m}/\mathrm{d}t$. Then, the current-induced spin–orbit torque can be given as $\mathbf{T}_{\mathrm{R}} = -J\mathbf{S}\times\mathbf{s}_{\mathrm{C}}$ with the localized spin $\boldsymbol{S} = \frac{M}{\gamma}\boldsymbol{m}$, which consists of a field-like component $\gamma H^{\mathrm{FL}}\mathbf{m}\times(\mathbf{j}\times\hat{z})$ and a damping-like component $\gamma H^{\mathrm{DL}}\mathbf{m}\times[\mathbf{m}\times(\mathbf{j}\times\hat{z})]$. Here, H^{FL} and H^{DL} represent the strengths of the current-induced field-like and damping-like effective fields, respectively.

A tight binding calculation was performed to study the magnetization dynamics of the Co film which was discretized into a square lattice. The lattice spacing was chosen to be a = 0.1 nm,[26,27] and hence the coupling strength between the neighbouring sites was $t = \frac{\hbar^2}{2m^*a} = 3.814$ eV, where $m^* \approx m_{\mathrm{e}} = 9.1\times10^{-31}$ kg is the effective mass. Here, the lattice spacing was set to be significantly smaller than the Fermi wavelength of Co to reduce the tight-binding dispersion to the quadratic one so that our model was a good approximation to simulate the Co film. For simplicity, the coupling between the leads and the central region was set to be $t_{\mathrm{L,R}} = 0.8t$. The Fermi energy was assumed to be that of the Co bulk which is 7.38 eV,[26] and the exchange energy was set to be J = 0.1 eV.[28] The temperature was fixed at 300 K. It was found that the Rashba constant α_{R} ranges from 4×10^{-11} to 3×10^{-10} eV m at the interfaces of heavy metal systems.[29,30] Therefore, we assumed $\alpha_{\mathrm{R}} = 10^{-10}$ eV m with the corresponding Rashba spin–orbit coupling $t_{\mathrm{so}} = \frac{\alpha_{\mathrm{R}}}{2a} = 0.5$ eV for the system without lateral structural asymmetry. The saturation magnitude of the Co layer is $M = 1.09\times10^{6}$ A m^{-1} from which the localized spin can be calculated through $S = MV/\gamma$. Here, V is the volume of the Co layer and $\gamma \approx \gamma_{\mathrm{e}} = 1.76\times10^{11}$ Hz T^{-1} is the gyromagnetic ratio which is assumed to be that of free electrons. The anisotropy energy was chosen to be $D = 8.3\times10^{-4}$ eV which corresponds to an effective magnetic field of B_{K} = 0.92 T in the z-direction.[9] The whole tight binding Hamiltonian can be found in the ESI.†

3. Results and discussion

Fig. 1(b) shows a calculated phase diagram of the minimum magnetic field required to switch the magnetization under different current densities and applied magnetic fields. Three regions are clearly manifested. In region I, it is found that the minimum magnetic field required by the magnetization switching does not depend on the current density and the reversal of magnetization occurs at the coercive field $|B_{\mathrm{c}}|$ = 0.84 T close to the anisotropic magnetic field, and this agrees with previous macrospin studies.[12,23] Once the current density exceeds 0.46×10^{8} A cm^{-2}, the system enters region II where the minimum external field required to switch the magnetization gradually decreases with increasing current density, which implies that the reversal of the magnetization is also assisted by the current-induced spin–orbit torque. The typical dynamics of the magnetization switching in the presence of both an applied bias and a magnetic field are presented in Fig. 1(c). Our numerical results show that when the magnetization approaches the xy plane, the spin–orbit torque nearly vanishes and this is the reason why an external field is still required to overcome the perpendicular magnetic anisotropy. Finally, the magnetization maintains precession after reversal. The behavior of the magnetization dynamics obtained by us agrees well with that of the experimental data.[10] It was also found that the reversal of magnetization is very fast. For instance, the switching time is about 80 ps for the case with $j = 5.5\times10^{8}$ A cm^{-2} and B_y = 0.4 T. In Region III, the coercivity almost vanishes when the current density exceeds 6.2×10^{8} A cm^{-2}. However, it is worth noting that a tiny external magnetic field along the current direction is still needed for a deterministic switching of magnetization.

In order to understand the switching of magnetization due to the spin–orbit torque in the absence of an external field, we propose two mechanisms directly due to structural asymmetry, as in ref. 15, induced by the variation of thickness, perpendicular to the transport direction, of the metal oxide (wedge-shaped) deposited on top of the ferromagnetic film, namely, the two mechanisms correspond to two different types of Rashba interaction whose physical origin will be discussed in the next section. The first type of Rashba interaction is of the form $g(x)(\hat{z}\times\mathbf{p})\cdot\boldsymbol{\sigma}$ with $g(x)$ as a linear function of x and $\mathbf{p}$ the electron momentum operator. In the tight binding representation, $g(x) = [\alpha_{\mathrm{R},0} + (\alpha_{\mathrm{R},x} - \alpha_{\mathrm{R},0})x/L]/2a$ where a is the lattice spacing and L is the sample size along the x direction. The second type of Rashba term is assumed to be $[\Delta\alpha_{\mathrm{R}}/2a](\hat{x}\times\mathbf{p})\cdot\boldsymbol{\sigma}$ to generate an additional field-like effective field $H_z^{\mathrm{FL}'}$ along the z-axis. The magnetization dynamics with the two different types of Rashba interactions were studied for the system under a current density of $j = 5.5\times10^{8}$ A cm^{-2}. Fig. 2(a) shows the reduction of the minimum magnetic field to achieve the switching of magnetization due to the first type of Rashba interaction. In the calculation, we fix $\alpha_{\mathrm{R},x0} = 0.5\times10^{-10}$ eV m at one side of the Co film and vary the Rashba constant $\alpha_{\mathrm{R},x}$ at the other side along the x-direction due to the Rashba term $g(x)(\hat{z}\times\mathbf{p})\cdot\boldsymbol{\sigma}$. The Rashba interaction in the absence of structural asymmetry was set to be $\alpha_{\mathrm{R}} = 10^{-10}$ eV m. It was found that the minimum field required to switch the magnetization decreases quadratically with an increasing gradient of the Rashba interaction along the x-direction. When we set the average Rashba constant along the x-axis to be same as that along the y-axis, namely, $\alpha_{\mathrm{R},x} = 1.5\times10^{-10}$ eV m, the minimum external field was found to be 0.33 T, which is smaller than that (0.4 T) of the case with a uniform Rashba constant as shown in Fig. 1(b). Once $\alpha_{\mathrm{R},x}$ exceeds 1.7×10^{-10} eV m with a Rashba

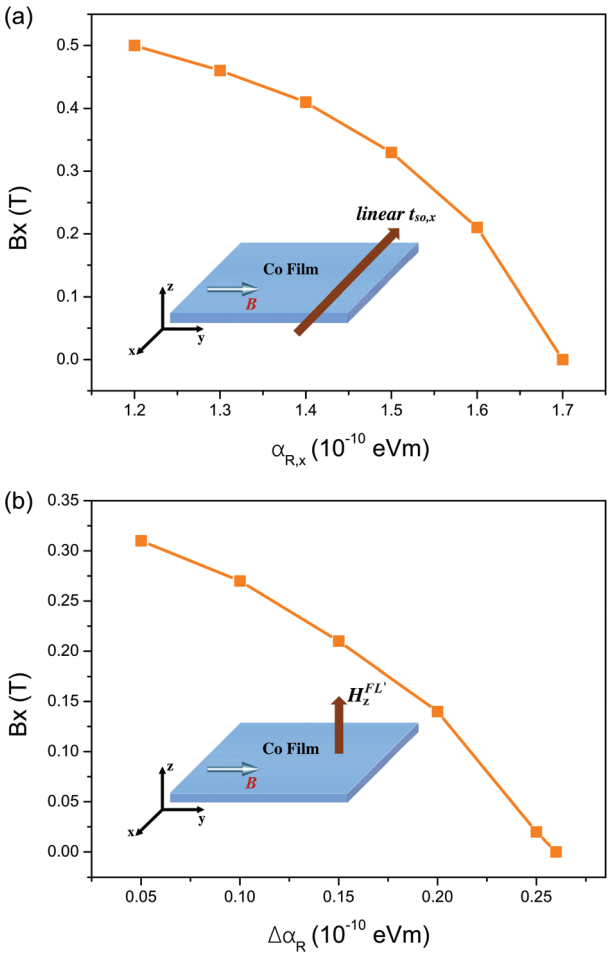

Fig. 2 (a) The minimum magnetic field required to reverse the magnetization with a linear Rashba constant along the *x*-axis with a different Rashba constant α_R at one side of the Co film. The Rashba constant at the other side was fixed to be 0.5×10^{-10} eV m. (b) The minimum magnetic field required to reverse the magnetization with an additional Rashba term $\Delta\alpha_R(\hat{x} \times \mathbf{p})\cdot\sigma$. The current densities of all system were set to be $j = 5.5 \times 10^8$ A cm^{-2}. Insets: schematic diagrams of the different spin–orbit interactions.

gradient $(\alpha_{R,x} - \alpha_{R,0})/L$ of 0.6 eV, the reversal of magnetization can be induced by an applied bias in the absence of an external field. We also propose a second Rashba interaction, motivated by the experimental results due to breaking structural symmetry.[15] Such a Rashba interaction can indeed assist magnetization reversal, as shown in Fig. 2(b). For instance, the minimum external field significantly decreases due to an increase of $\Delta\alpha_R$, and it reduces to 0.31 T when we add a very small Rashba interaction with $\Delta\alpha_R = 5 \times 10^{-12}$ eV m. Once $\Delta\alpha_R$ reaches 2.6×10^{-11} eV m, the magnetization switching is dominated by the current-induced spin–orbit torque without the assistance of the external field, which is in agreement with an experimental report of switching in the absence of magnetic fields.[15] In the following, we will show that both mechanisms are rooted in the same origin, *i.e.*, the structural asymmetry of the system.

We have studied two systems with or without structural asymmetry along the *x*-direction. For the latter system, what we found is as follows. At the beginning stage of the magnetization dynamics where **M** was mainly along the *z*-direction, the current-induced torque originated from the spin–orbit field and the external magnetic field is the main contributor for the reversal of magnetization. The torque from the anisotropy field was relatively small and did not contribute much to the magnetization switching. Our numerical results show that at this stage, the effective spin–orbit field $\mathbf{H}_R$ almost points to the *x*-direction. As a result, the spin–orbit torque $\mathbf{T}_R \sim \mathbf{H}_R \times \mathbf{M}$ almost points to the *y*-direction which agrees with the semi-classical theory for Rashba torque.[5] Combined with the external magnetic field, the action of the current on the magnetization can be considered as an effective perpendicular field $\mathbf{B}_z \approx \mathbf{H}_R \times \mathbf{B}_y$.[10] With the assistance of this effective perpendicular field, the magnetization starts to go downward. The field-like (H^{FL}) and damping-like (H^{DL}) components of the current-induced effective spin–orbit field are plotted in Fig. 1(d). We see that when the magnetization remains in the upper hemisphere, both the field-like and damping-like effective fields give torques with $-z$ components to help switch the magnetization. It was found that H^{FL} increases rapidly once an external bias is applied while H^{DL} increases first and then starts to decrease, indicating that the field-like effective field contributes more significantly to the magnetization switch. Once **M** goes across the *xy* plane, H^{FL} and H^{DL} start to oscillate around about 30 mT and −30 mT at approximately 90 ps, respectively. The magnetization then processes in the lower hemisphere due to the competition between the damping-like and field-like effective fields.

Concerning the Rashba spin–orbit interaction in the system with lateral structural asymmetry, we would like to understand the nature of the magnetization switching in the absence of an external field, in particular, the origin of the two mechanisms discussed above. Since the Rashba interaction is proportional to the potential gradient, we first calculated the potential barrier of the ferromagnetic film as a function of the thickness of the metal oxide using density functional theory (DFT). In our simulation, the Co film was sandwiched between different layers of TaO and 4 atomic layers of Ta along the *z*-direction, as shown in the inset of Fig. 3. The DFT calculations were performed using the projector augmented wave method as implemented in the Vienna *ab initio* simulation package.[31,32] The exchange and correlation were approximated using the generalized gradient approximation (GGA) with the Perdew–Burke–Ernzerhof (PBE) functional.[33] A plane-wave basis set with the kinetic energy cutoff of 450 eV was employed. The 3×3 supercell of TaO and 4×4 supercells of Co and Ta were used to match the lattice constant. We use 4 atomic layers for both Co and Ta films in the simulation box. The *k*-mesh of $3 \times 3 \times 1$ was chosen to sample the first Brillouin zone.

Fig. 3 shows that the potential, *V*, at the interface between the TaO and Co films increases monotonically with the thickness, *d*, of the TaO film. For qualitative discussion, we assume that the interfacial potential, *V*, has linear dependence on *d* so

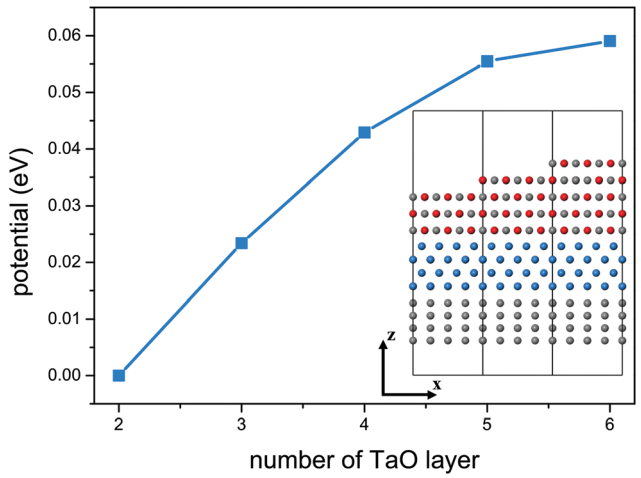

Fig. 3 Potential at the interface between TaO and Co films with different numbers of atomic layers of TaO calculated using DFT. The interfacial potential for the system with 2 atomic layers of TaO was set to be zero as the reference. Inset: schematic diagram of a Co film sandwiched between TaO films with different atomic layers and Ta films. The gray, red, and blue balls represent the Ta, O, and Co atoms, respectively.

that when a wedge-shaped TaO layer is deposited on the Co films of the TaO/Co/Ta device, the interfacial potential, V, will depend on x in a linear fashion $V(x) = a_1x + b_1$, from which we have $\nabla_x V = a_1\hat{x}$. The potential gradient along the z-direction is estimated to be $\nabla_z V = \frac{V(x) - V_0}{l_z}\hat{z}$ where V_0 is the potential at the interface between the Co and Ta films and l_z is the thickness of the Co film. Therefore, from the definition of the Rashba interaction $H_{so} \propto (\nabla V \times \mathbf{p})\cdot\boldsymbol{\sigma}$,[34] we find two contributions: (1) $g(x)(\hat{z} \times \mathbf{p})\cdot\boldsymbol{\sigma}$ with $g(x)$ as a linear function of x, and (2) $(\hat{x} \times \mathbf{p})\cdot\boldsymbol{\sigma}$. We see that the two scenarios studied in Fig. 2(a) and (b) naturally arise from the wedge-shaped TaO layer. Note that both Rashba interactions break the mirror symmetry along the transverse direction (x-direction) which agrees with the symmetry-based argument discussed in ref. 15. It is worth noting that the oxygen content of the metal oxide is non-uniform due to the varied thicknesses in experiments[15] which would further affect the interfacial potential.

4. Conclusions

In summary, we have developed a microscopic theory to understand the phenomenon of magnetization switching due to spin–orbit torque in a system with lateral structural asymmetry without an external magnetic field. In particular, to understand the effect of wedge-shaped metal oxide on the magnetization switching, two different types of Rashba interactions were proposed due to the potential profile along the transverse direction at the interface between the metal oxide and the ferromagnetic film obtained from DFT calculations. It was found that the minimum external field required to reverse the magnetization can be reduced to zero by either type of Rashba interaction of the form (1) $g(x)(\hat{z} \times \mathbf{p})\cdot\boldsymbol{\sigma}$ with $g(x)$ as a linear function or (2) $(\hat{x} \times \mathbf{p})\cdot\boldsymbol{\sigma}$. To simulate magnetization switching due to these Rashba interactions, we have developed a stochastic LLG equation using the non-equilibrium Green's function technique and studied the magnetization dynamics due to the spin–orbit torque of the ferromagnetic films from the perspective of quantum transport. Three regions were clearly manifested for the current assisted magnetization reversal in the presence of an external magnetic field. At the beginning of the magnetization switching, the current-induced spin–orbit torque almost points perpendicular to the transport direction, which agrees with the semiclassical theory. Our simulations provide physical explanations for the experimental observations of the reversal of magnetization in the absence of an external field with the lateral structural asymmetry of devices.[15]

It is worth mentioning that the Edelstein effect was mainly considered in our simulation which produces a transverse nonequilibrium spin density along the x-direction and then generates a field-like torque. Recently, the spin Hall torque induced by the spin Hall effect has been extensively studied in the current-induced magnetization switching in ferromagnetic layers.[12,13,18] The spin Hall torque acts predominantly as a damping-like torque and its magnitude greatly depends on the spin Hall angle of heavy metals and the interface conductances between ferromagnets and heavy metals. If one can obtain the tight-binding Hamiltonian of a heavy metal/ferromagnet interface fitted to the electronic structures from first principles studies, this can be combined with our theory to study the spin–orbit and spin Hall torques simultaneously in a three-dimensional device with at least four probes.

Conflicts of interest

There are no conflicts to declare.

Acknowledgements

This work was financially supported by the National Natural Science Foundation of China (Grant No. 11704190 and 11704232), the Research Grant Council (Grant No. HKU 17311116), the University Grant Council (Contract No. AoE/P-04/08) of the Government of HKSAR, and the Jiangsu Provincial Natural Science Foundation of China (Grant No. BK20171030).

References

1 E. B. Myers, D. C. Ralph, J. A. Katine, R. N. Louie and R. A. Buhrman, *Science*, 1999, **285**, 867–870.
2 C. Chappert, A. Fert and F. N. Van Dau, *Nat. Mater.*, 2007, **6**, 813–823.
3 A. Brataas, A. D. Kent and H. Ohno, *Nat. Mater.*, 2012, **11**, 372–381.

4 D. Ralph and M. Stiles, *J. Magn. Magn. Mater.*, 2008, **320**, 1190–1216.
5 A. Manchon and S. Zhang, *Phys. Rev. B: Condens. Matter Mater. Phys.*, 2008, **78**, 212405.
6 A. Manchon and S. Zhang, *Phys. Rev. B: Condens. Matter Mater. Phys.*, 2009, **79**, 094422.
7 I. Garate and A. H. MacDonald, *Phys. Rev. B: Condens. Matter Mater. Phys.*, 2009, **80**, 134403.
8 P. M. Haney and M. D. Stiles, *Phys. Rev. Lett.*, 2010, **105**, 126602.
9 I. M. Miron, G. Gaudin, S. Auffret, B. Rodmacq, A. Schuhl, S. Pizzini, J. Vogel and P. Gambardella, *Nat. Mater.*, 2010, **9**, 230–234.
10 I. M. Miron, K. Garello, G. Gaudin, P.-J. Zermatten, M. V. Costache, S. Auffret, S. Bandiera, B. Rodmacq, A. Schuhl and P. Gambardella, *Nature*, 2011, **476**, 189–193.
11 L. Liu, C.-F. Pai, Y. Li, H. W. Tseng, D. C. Ralph and R. A. Buhrman, *Science*, 2012, **336**, 555–558.
12 L. Liu, O. J. Lee, T. J. Gudmundsen, D. C. Ralph and R. A. Buhrman, *Phys. Rev. Lett.*, 2012, **109**, 096602.
13 K. Garello, I. M. Miron, C. O. Avci, F. Freimuth, Y. Mokrousov, S. Blügel, S. Auffret, O. Boulle, G. Gaudin and P. Gambardella, *Nat. Nanotechnol.*, 2013, **8**, 587–593.
14 Y. Fan, P. Upadhyaya, X. Kou, M. Lang, S. Takei, Z. Wang, J. Tang, L. He, L.-T. Chang, M. Montazeri, *et al.*, *Nat. Mater.*, 2014, **13**, 699–704.
15 G. Yu, P. Upadhyaya, Y. Fan, J. G. Alzate, W. Jiang, K. L. Wong, S. Takei, S. A. Bender, L.-T. Chang, Y. Jiang, *et al.*, *Nat. Nanotechnol.*, 2014, **9**, 548–554.
16 X. Zhao, W. Liu, S. Li, T. Wang, L. Liu, Y. Song, S. Ma, X. Zhao and Z. Zhang, *Nanoscale*, 2018, **10**, 7612–7618.
17 Y. Sheng, K. W. Edmonds, X. Ma, H. Zheng and K. Wang, *Adv. Electron. Mater.*, 2018, **4**, 1800224.
18 M. Yang, K. Cai, H. Ju, K. W. Edmonds, G. Yang, S. Liu, B. Li, B. Zhang, Y. Sheng, S. Wang, *et al.*, *Sci. Rep.*, 2016, **6**, 20778.
19 Y.-W. Oh, S.-h. C. Baek, Y. Kim, H. Y. Lee, K.-D. Lee, C.-G. Yang, E.-S. Park, K.-S. Lee, K.-W. Kim, G. Go, *et al.*, *Nat. Nanotechnol.*, 2016, **11**, 878.
20 K. Cai, M. Yang, H. Ju, S. Wang, Y. Ji, B. Li, K. W. Edmonds, Y. Sheng, B. Zhang, N. Zhang, *et al.*, *Nat. Mater.*, 2017, **16**, 712.
21 J. Foros, A. Brataas, Y. Tserkovnyak and G. E. W. Bauer, *Phys. Rev. Lett.*, 2005, **95**, 016601.
22 J. Swiebodzinski, A. Chudnovskiy, T. Dunn and A. Kamenev, *Phys. Rev. B: Condens. Matter Mater. Phys.*, 2010, **82**, 144404.
23 D. Wang, *Appl. Phys. Lett.*, 2012, **100**, 212405.
24 Y. Utsumi and T. Taniguchi, *Phys. Rev. Lett.*, 2015, **114**, 186601.
25 X. Zhang, C. Wang, Y. Liu, Z. Zhang, Q. Jin and C.-G. Duan, *Sci. Rep.*, 2016, **6**, 18719.
26 M. Wawrzyniak, M. Mackowski, Z. Sniadecki, B. Idzikowski and J. Martinek, *Acta Phys. Pol., A*, 2010, **118**, 375.
27 N. L. Chung, M. B. A. Jalil and S. G. Tan, *AIP Adv.*, 2012, **2**, 022165.
28 M. Pajda, J. Kudrnovský, I. Turek, V. Drchal and P. Bruno, *Phys. Rev. B: Condens. Matter Mater. Phys.*, 2001, **64**, 174402.
29 J. Henk, M. Hoesch, J. Osterwalder, A. Ernst and P. Bruno, *J. Phys.: Condens. Matter*, 2004, **16**, 7581.
30 C. R. Ast, J. Henk, A. Ernst, L. Moreschini, M. C. Falub, D. Pacilé, P. Bruno, K. Kern and M. Grioni, *Phys. Rev. Lett.*, 2007, **98**, 186807.
31 G. Kresse and J. Furthmüller, *Phys. Rev. B: Condens. Matter Mater. Phys.*, 1996, **54**, 11169–11186.
32 G. Kresse and D. Joubert, *Phys. Rev. B: Condens. Matter Mater. Phys.*, 1999, **59**, 1758–1775.
33 J. P. Perdew, K. Burke and M. Ernzerhof, *Phys. Rev. Lett.*, 1996, **77**, 3865–3868.
34 Q.-f. Sun, J. Wang and H. Guo, *Phys. Rev. B: Condens. Matter Mater. Phys.*, 2005, **71**, 165310.